Challenge Journal of Structural Mechanics

Research Article

Moment-rotation behavior of semi-rigid web cleat connections

Merve Sağıroğlu [a], Mahyar Maali [a], Abdulkadir Cüneyt Aydın [b,*], Mahmut Kılıç [b]

[a] *Department of Civil Engineering, Erzurum Technical University, 25050 Erzurum, Turkey*
[b] *Department of Civil Engineering, Atatürk University, 25240 Erzurum, Turkey*

ABSTRACT

The behavior of beam-column semi-rigid connection plays an important role in the response of a steel moment resisting, stiffness and rotation capacity framed structure, especially under static loading conditions. In this study, the moment-rotation characteristics of semi-rigid bolted connections using web cleat connections with IPE standard profile is discussed, based on the experimental investigation. The study revealed that the moment resistance of beam-column semi-rigid connection is improved by increasing the height of the beam to the height of web cleat joint (H), and the increasing thickness of web and flange in web cleat joints. The aim was to provide necessary data to improve the Eurocode 3 and efficiently use residue IPE standard profiles, rather than send them back to the consumption cycle. While the resistance moment increased with an increase in H from H_{min} to H_{max}.

ARTICLE INFO

Article history:
Received 8 January 2020
Revised 3 February 2020
Accepted 24 February 2020

Keywords:
Moment-rotation curve
Semi-rigid connection
Web cleat connection
Joint
Rotation capacity
Eurocode 3

1. Introduction

Experimental tests can be used to obtain the moment-rotation curve of beam-column joints, but it is too expensive for everyday design. The behavior of beam-column semi-rigid connection plays an important role in the response of a steel moment resisting, stiffness and rotation capacity framed structure, especially under static loadings. The use of semi-rigid connections provides a good response under static loadings. It is necessary to consider the behavior of connections in the design and analysis of steel frames because it represents the actual behavior (Sağıroğlu and Aydin, 2015). In addition to considering the behavior of connections in the main axes, some researchers (Lima et al., 2002) considered the behavior of minor axis beam-to-column connections. In the last decade, many researchers were carried out to study the behavior of semi-rigid web cleat connections. Table 1 presents some experimental research of beam-column web cleat connections. T-shaped combinations created using the IPE standard profile and T-shaped elements are different from those in the literature, which utilize welded plates. Thus, the elimination of the problems occurring at the welds of connections such as the occurrence of fracture points and the inability to perform well in place is expected. To recommend the use of weld-less T connections, a knowledge of their behavior is needed. However, web cleat connections that use the IPE standard profile are not mentioned and investigated in either Eurocode 3 or the literature, as in this research (Eurocode 3 investigated cleat leg connections in the section bolted T-stubs). Thus, the aim of this study was to analyze the influence of T connections that utilize the IPE standard profile and the height of beam to height of web cleat joint (H) of web cleat joints on the behavior of steel connections, to provide the necessary data to improve Eurocode 3 (section 3.5.2. Bolted T-stubs which investigated cleat leg connections) and efficiently use residue IPE standard profiles, rather than send them back to the consumption cycle. Moment-rotation curves were used to predict the main characteristics of the relevant connections, such as the resistance moment, the rotation capacity, the stiffness, and the energy dissipation.

2. Experimental Investigation

2.1. Specimens

The experimental program is presented in Fig. 1 and Table 2. This paper presents, the nine experimental

* *Corresponding author*. Tel.: +90-442-231-4781 ; Fax: +90-442-231-4910 ; E-mail address: acaydin@atauni.edu.tr (A. C. Aydın)
ISSN: 2149-8024 / DOI: https://doi.org/10.20528/cjsmec.2020.03.002

models were developed to predict of the behavior of bolted web cleat semi-rigid connections with IPE standard profile under statically loaded in three groups: C300, C270, and C240 groups (C300 cut from of IPE300 standard Profile, C270 cut from of IPE270 standard Profile, and C240 cut from of IPE240 standard Profile). The behaviors of the web cleat joints were compared within their groups (C300-H_{max}, C300-H_{min}, C300-H_{av}, C270-H_{max}, C270-H_{min}, C270-H_{av}, C240-H_{max}, C240-$H_{min,}$ and C240-H_{av}) (H = height of beam to height of web cleat joint). Column stiffeners with a thickness equal to 10 mm were welded to the column by means of a continuous 45° fillet weld. Thus, columns with a large cross-section were chosen, and the use of the stiffener prevented excessive deflection in the flange column (Maali et al., 2017). The plate stiffener was S355 and web cleat profile, and the steel type was S235. HE160B was used for the columns, and IPE240 was selected for the beams. Hand-tightened full-threaded grade 8.8 M14 bolts in 16-mm drilled holes were used consistently for all the tested specimens. The aim of this study was to analyze the influence of T connections that utilize the IPE standard profile and the height of beam to height of web cleat joint (H) of web cleat joints on the behavior of steel connections, to provide the necessary data for improving Eurocode 3 (section 3.5.2. Bolted T-stubs which investigated cleat leg connections) and efficiently use residue IPE standard profiles, rather than send them back to the consumption cycle.

2.2. Material properties

The coupon tension test of the column stiffener, web cleat profile, column, flange and web of the beam, and the mechanical properties of the bolt material were performed in accordance with the relevant standards (UNE-EN 10002-1, 2002). The characteristic of steels and bolts (8.8) are presented in Table 3.

2.3. Test setup

The applied force is static and applied by a 900 kN hydraulic jack with 300 mm maximum piston stroke and a constant displacement speed of 0.01 mm/s until the collapse. To prevent the torsion of the beam, a two-column guide close to the beam was used (Aydın et al., 2015a, 2015b). Merely, the experiments did not exhibit lateral torsion. The testing equipment is shown in Fig. 2. According to relevant given literature, and to obtain more realistic behavior with the specific testing machine the beam and column lengths are chosen as 1500 mm (Aydın et al., 2015a, 2015b).

The main requirements for the instrumentation were measurements of (1) the applied load (P), which was measured using a load cell and hydraulic pump; (2) the displacements (DT) of the connection, beam, web cleat joint, and flange of the column, which were measured using linear variable displacement transducers (LVDT) with a maximum displacement of 100 mm (Figs. 2,3); and the strains at the web cleat connections, which were measured using strain gauges (TML YEFLA-5 (a maximum strain of 15%–20%)) (Maali et al., 2012, 2018, 2019; Fatemi et al., 2013; Niloufari et al., 2014). A data logging device recorded all of the measurements and load cell values at 1-s intervals during the tests. Four strain gauges (ST) were added to the web cleat connection, to observe the strain distribution (Fig. 1). All of the tests used the same arrangement for the locations of the strain gauges and measuring devices.

Nomenclature

h	Height of web cleat joint
h_y	Height of the beam without thickness of flange
H	Web cleat ratio (h_y/h)
F_u	Ultimate or tensile stress
F_y	Yield stress
E_{st}	Strain hardening modulus
$\rho_y=f_y/f_u$	Yield ratio
ε_{st}	Strain at the strain hardening point
ε_{uni}	Uniform strain
ε_f	Strain at rupture load,
X	Cartesian axis; distance
E	Young's modulus
I	Moment of inertia
M	Bending moment
$M_{j.Rd}$	Joint flexural plastic (design) resistance
$M_{j.\max}$	Maximum bending moment
$M_{\min.K-R}$	Lower resistance bound of the knee-range of the joint moment-rotation curve
$M_{\sup.K-R}$	Upper resistance bound of the knee-range of the joint moment-rotation curve
$M_{\Theta.Cd}$	Bending moment at fracture of the joint
P	Concentrated force
$S_{j.ini}$	Initial rotational stiffness of a joint
$S_{j.p-1}$	Post-yield rotational stiffness of a joint
Θ_{Cd}	Rotation capacity of a connection
$\Theta_{Mj.\max}$	Rotation of the connection at maximum load
$\Theta_{M.j.Rd}$	Connection rotation analytical value at which the moment resistance first reaches $M_{j.Rd}$
$\Theta_{\min.K-R}$	Rotation between the lower bound of the knee-range of the joint moment-rotation curve and the rotation capacity
$\Theta_{\sup.K-R}$	Rotation between the upper bound of the knee-range of the joint moment-rotation curve and the rotation capacity
$\Psi_{j.\max\ load}$	Joint ductility index evaluated for the rotation at maximum load
Ψ_j	Joint ductility index
Θ	Rotation
DT_i	LVDT
ST_i	Strain gauge

Table 1. Beam-column web cleat connections.

Author(s) and Year	Explanation	Experimental number
Coelho et al. (2004)	Experimental assessment of the behavior of bolted T-stub connections made up of welded plates	32
Piluso and Rizzano (2008)	Experimental analysis and modeling of bolted T-stubs under cyclic loads	1

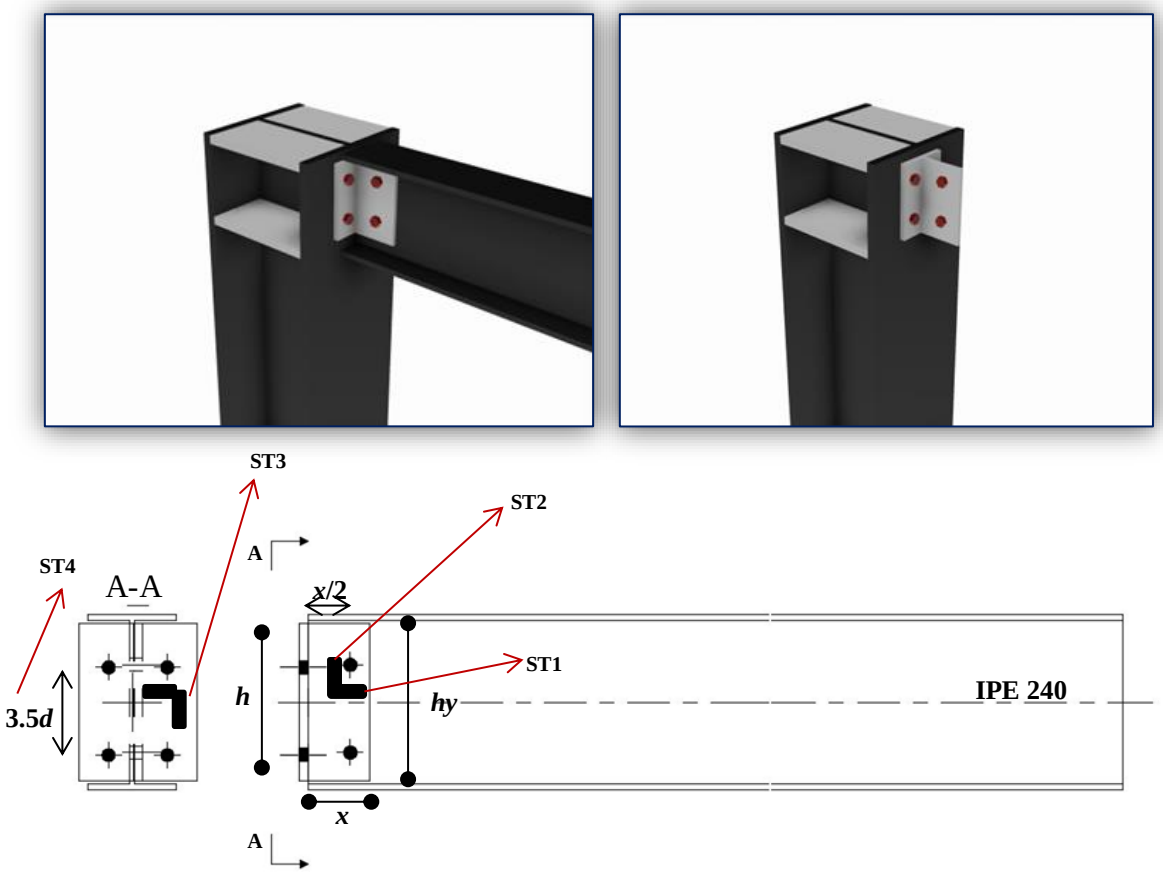

Fig. 1. Web cleat geometry, proposed semi-rigid connection, and locations of strain gauges (ST1 = parallel to beam on Web cleat; ST2 = perpendicular to beam on Web cleat; ST3 = parallel to the column on Web cleat; ST4 = perpendicular to the column on Web cleat; *d* = diagonal to bolts).

Table 2. Test details.

Groups Name	Experiment	Web cleat joint	$H_{max}=hy_{max}/h$	$H_{min}=hy_{min}/h$	$H_{av}=Hy_{av}/h$	X (mm)
C300 group	C300-H_{max}	IPE 300	1	-	-	89
	C300-H_{min}		-	0.63	-	
	C300-H_{av}		-	-	0.82	
C270 group	C270-H_{max}	IPE 270	1	-	-	
	C270-H_{min}		-	0.63	-	
	C270-H_{av}		-	-	0.82	
C240 group	C240-H_{max}	IPE 240	1	-	-	
	C240-H_{min}		-	0.63	-	
	C240-H_{av}		-	-	0.82	

h_y=height of the beam without the thickness of the flange, h=height of Web cleat joint, av= average, max=maximum, min= minimum, x=length of Web cleat connection.

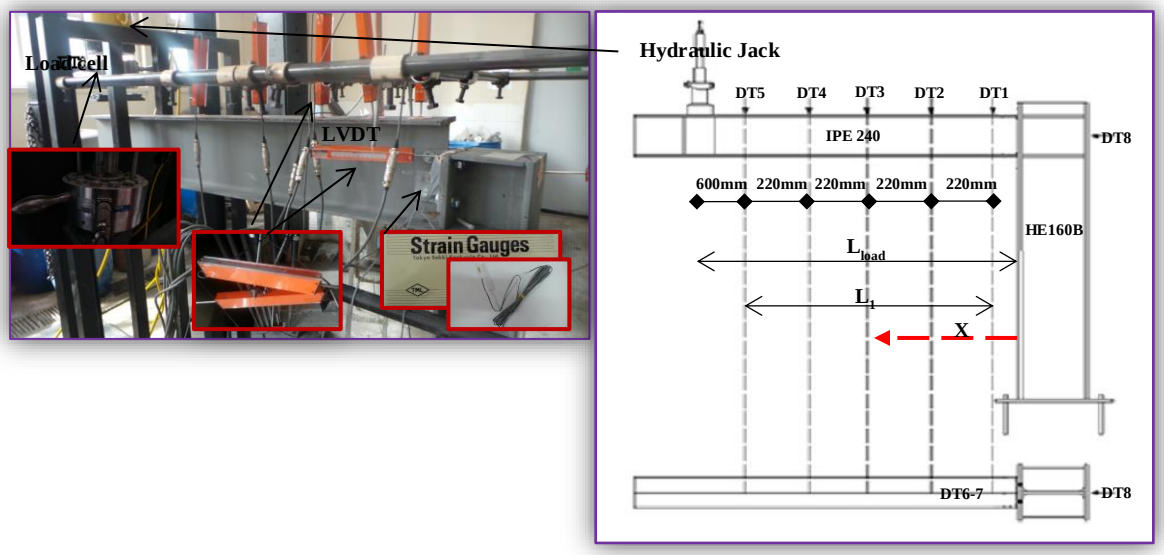

Fig. 2. Test set-up.

Table 3. Average characteristic values for structural steels and bolt (8.8).

	E (MPa)	E_{st} (MPa)	f_y (MPa)	f_u (MPa)	$\rho_y = f_y/f_u$	ε_{st}	ε_{uni}	ε_f
10 mm plate	205352	1798	687	721	0.95	2.71×10^{-2}	2.68×10^{-2}	1.62×10^{-1}
Bolt	-----	-----	1127	1247	0.90	-----	-----	-----
Beam Web	203521	1374	521	649	0.80	1.81×10^{-2}	1.59×10^{-2}	1.09×10^{-1}
Beam Flange	204399	1399	562	685	0.82	1.97×10^{-2}	1.68×10^{-2}	1.15×10^{-1}
Column Web	204424	1396	541	637	0.85	1.89×10^{-2}	1.63×10^{-2}	1.11×10^{-1}
Column Flange	208242	1928	831	945	0.88	2.99×10^{-2}	2.81×10^{-2}	1.78×10^{-1}
T300-stub web	204121	1425	581	705	0.82	2.18×10^{-2}	1.80×10^{-2}	1.38×10^{-1}
T300-stub Flange	204781	1499	638	735	0.87	2.43×10^{-2}	1.99×10^{-2}	1.69×10^{-1}
T270-stub web	204001	1394	545	671	0.81	1.90×10^{-2}	1.66×10^{-2}	1.13×10^{-1}
T270-stub Flange	204498	1428	588	702	0.84	2.00×10^{-2}	1.70×10^{-2}	1.21×10^{-1}

E= the Young's modulus, E_{st}= the strain hardening modulus, f_y= the static yield, f_u= tensile stresses, ε_{st}= the strain at the strain hardening point, ε_{uni}=the uniform strain, ε_f= the strain at rupture load.

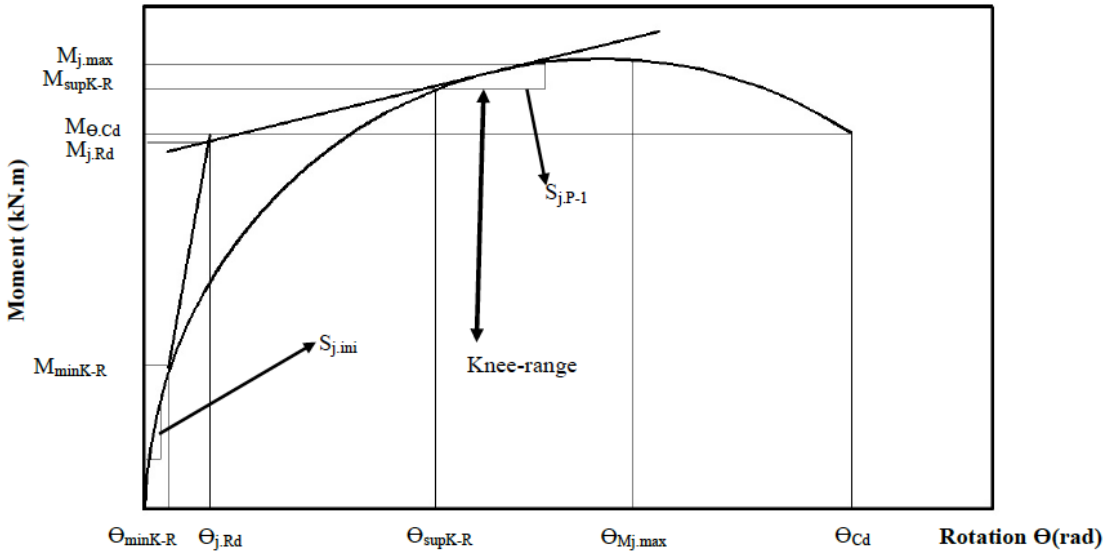

Fig. 3. Typical moment-rotation curve.

The designed connections form various moment-rotation curves that describe the relationship between the applied moment (M) and the corresponding rotation (θ) (Sağıroğlu and Aydin, 2015). The bending moment (M) and the rotation are predicted by using displacements of the beam or top-and-seat angle connection as given below formulation:

$$M = P\,L_{load} \tag{1}$$

The rotational deformation of the joint (θ) is equal to the connection rotation. The beam rotation is approximately given by (Fig. 2.):

$$\theta = \frac{arctan\left(\delta_{DT1}-\delta_{DT5}-\left(-\frac{P}{EI}\right)\left(\frac{X_{DT1}^3}{6}-\frac{L_{load}X_{DT1}^2}{2}\right)\right)}{L1} \tag{2}$$

where I is the moment of inertia and E is Young's modulus of the beam. All deformations values presented throughout the remainder of the section refer to the readings from DT1 (Maali et al., 2015, 2017).

3. Eurocode 3: Moment-rotation curve

The M–θ curve of the connection may be described by using the aforementioned relationships. The main features are the plastic flexural resistance, $M_{j.Rd}$, which corresponds to the intersection point of the previous two regression lines obtained for the initial stiffness ($S_{j.ini}$) and for the post-limit stiffness ($S_{j.p-l}$) and its corresponding rotation $\theta_{M.Rd}$; the maximum bending moment, $M_{j.\max}$, and its corresponding rotation, $\theta_{M.j.\max}$; The knee-range of the M–θ curve, which is defined as the transition zone between the initial and post-limit stiffness, with its lower boundary at $M_{\min k-R}$ and rotation $\theta_{\min k-R}$, and with its upper limit at $M_{\sup k-R}$ and rotation $\theta_{\sup k-R}$; The bending moment capacity, $M_{\theta.Cd}$, and its corresponding rotation capacity, θ_{cd}. In particular, the following characteristics were assessed for the different experimental tests (UNE-EN 10002-1, 2002; Maali et al., 2016; Sağıroğlu et al., 2018), as drawn in Fig. 3:

The ductility of a joint (Ψ_j) reflects the length of the yield plateau of the moment-rotation response. The proposed definition of the ductility of a joint is the difference between the rotation corresponding to the joint plastic resistance, θ_{MRd}, and the total rotation capacity, θ_{Cd} (Schleich et al. 1998; Gil et al., 2003) (Fig. 3). Thus, the joint ductility relates the maximum rotation of the joint, θ_{Cd}, to the rotation corresponding to the joint's plastic flexural resistance, θ_{MRd} (UNE-EN 10002-1, 2002; Piluso and Rizzano, 2008):

$$\Psi_j = \frac{\theta_{Cd}}{\theta_{MRd}} \tag{3}$$

Also, the rotation values at the maximum load and corresponding ductility, $\Psi_{j.\max\ load}$, can be derived from:

$$\Psi_{j.\max\ load} = \frac{\theta_{Mj.\max}}{\theta_{MRd}} \tag{4}$$

Eurocode 3 (2005) gives quantitative rules to obtain the joint flexural plastic resistance and initial rotational stiffness for major beam-to-column joints of end-plate connections. These properties are evaluated below using the geometric and mechanical nominal properties in the Eurocode 3 (Gil et al., 2003).

4. Results and Discussion

The moment-rotation responses for the nine full-scale specimens of steel-bolted, beam-to-column connections with web cleat joints in three groups are reported in Fig. 4 and listed in Tables 4 and 5. Showed that percent of the H characters of all models.

Table 4. Moment–rotation characteristics.

Group	Experiment	KR (knee-range)	Resistance (kN.m)			Stiffness (kN.m/rad)			Rotation (rad)					Ψ_j	$\Psi_{j.\max\ load}$	Energy Dissipated (kN.m.rad)
			$M_{j.Rd}$	$M_{j.\max}$	$M_{\theta Cd}$	$S_{j.ini}$	$S_{j.p-l}$	$S_{j.ini}/S_{j.p-l}$	$\theta_{M.Rd}$	$\theta_{Min.K.R}$	$\theta_{M\sup.k.R}$	$\theta_{Mj.\max}$	Θ_{Cd}			
C300	C300-$H_{\max}$	1.67-8.34	4.93	10.3	10.29	1.82	0.39	4.64	0.019	0.0057	0.063	0.09	0.09	4.79	4.79	0.47
	C300-$H_{\min}$	1.79-8.56	4.64	10.1	10.14	0.74	0.63	1.18	0.062	0.033	0.12	0.14	0.14	2.23	2.23	0.70
	C300-H_{av}	1.13-7.85	3.89	10.1	9.96	1.03	0.52	1.99	0.034	0.0083	0.099	0.13	0.14	4.06	3.94	0.70
C270	C270-$H_{\max}$	0.28-9.76	7.68	11.3	11.17	0.95	0.52	1.84	0.039	0.00002	0.055	0.07	0.07	1.79	1.74	0.39
	C270-$H_{\min}$	0.28-10.77	5.44	11.2	11.19	1.04	0.59	1.76	0.049	0.0014	0.12	0.13	0.13	2.55	2.55	0.70
	C270-H_{av}	2.02-6.62	4.91	7.84	7.8	9.3	0.28	33.29	0.006	0.0027	0.065	0.10	0.11	17.67	17	0.42
C240	C240-$H_{\max}$	0.88-9.33	2.99	10.6	9.96	2.87	0.64	4.44	0.011	0.000016	0.098	0.11	0.12	10.73	10.45	0.63
	C240-$H_{\min}$	1.23-9.04	4.07	9.97	9.61	1.39	0.58	2.41	0.024	0.0087	0.094	0.10	0.11	4.463	4.30	0.53
	C240-H_{av}	0.47-7.59	4.4	9.06	7.7	1.52	0.63	2.41	0.031	0.0022	0.08	0.099	0.11	3.55	3.19	0.50

Table 5. Percent of the H characteristics of all models.

Group	Experimental	$(M_{j.Rd}\,(H_{max})$- $M_{j.Rd}\,(H_{min}$ and $H_{av}))/$ $M_{j.Rd}\,(H_{max})$	$(M_{j.max}\,(H_{max})$- $M_{j.max}\,(H_{min}$ and $H_{av}))/$ $M_{j.max}\,(H_{max})$	$(\theta_{M.Rd}\,(H_{max})$- $\theta_{M.Rd}\,(H_{min}$ and $H_{av}))/$ $\theta_{M.Rd}\,(H_{max})$	$(\theta_{Mj.max}\,(H_{max})$- $\theta_{Mj.max}\,(H_{min}$ and $H_{av}))/$ $\theta_{Mj.max}\,(H_{max})$	$(\Psi_j\,(H_{max})$- $\Psi_j\,(H_{min}$ and $H_{av}))/$ $\Psi_j\,(H_{max})$	$(\Psi_{j.max\ load}\,(H_{max})$- $\Psi_{j.max\ load}\,(H_{min}$ and $H_{av}))/$ $\Psi_{j.max\ load}\,(H_{max})$
C300	C300-H_{max}	-	-	-	-	-	-
	C300-H_{min}	21	1	69	-	54	54
	C300-H_{av}	6	-	45	3	15	18
C270	C270-H_{max}	-	-	-	-	-	-
	C270-H_{min}	36	31	88	-	-	-
	C270-H_{av}	29	1	20	18	86	86
C240	C240-H_{max}	-	-	-	-	-	-
	C240-H_{min}	-	15	-	-	67	70
	C240-H_{av}	8	6	54	4	59	59

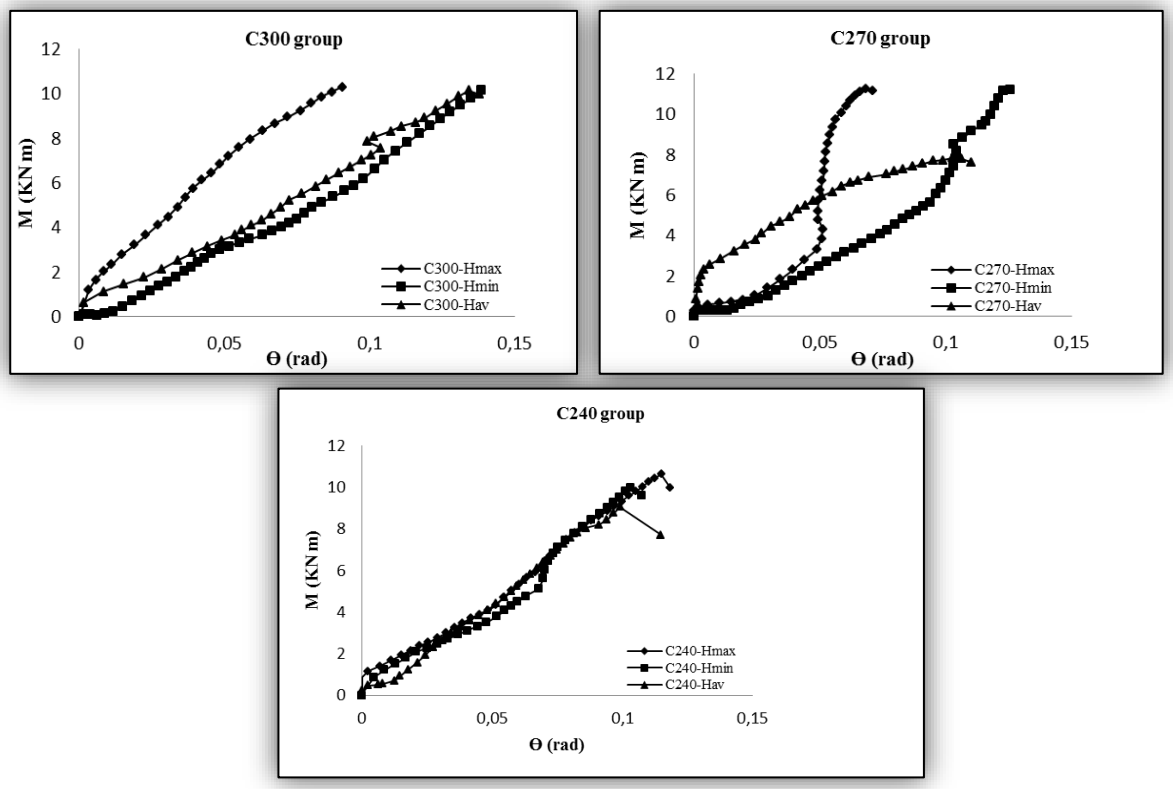

Fig. 4. Moment-rotation curves for three groups.

These curves and tables showed that:

The increasing web cleat ratio (H) increased the plastic flexural resistance about 6%-21%, 29%-36%, and 8%, for all the models. Furthermore, the thickness increase of the joints (from C270 to C300), increased the plastic flexural resistance about 39%–61%, 12%–25%, and 10%, also.

The maximum bending moments of all models increased about 1%, 1%–31%, and 6%–15%, with an increase in the web cleat ratio from H_{min} to H_{max}. Furthermore, the increasing joint thickness (C270 to C300 group of models), increased the maximum bending moments about 6%, 2%–11% and 11%–23%, also. Likewise, the bending moment capacities are increased with the increasing web cleat ratio and joint thickness.

As mentioned above, increasing web cleat ratio, also increased the initial to post-limit stiffness ratio about 41%-75%, 4%-95%, and 46%, for the models C300, C270, and C240, respectively. Moreover, the initial to post-limit stiffness ratios are increased about 4%–60% and 93%, for the increasing joint thickness (C270 to C300). Generally, the rate of the initial stiffness to the post-limit stiffness increased with an increase in the H from H_{min} to H_{max}.

The rotations of the plastic flexural resistance for the C300, C270, and C240 groups decreased by about 45%–69%, 20%–88%, and 54%, respectively, with an increase in H from H_{min} to H_{max}. The rotations of the plastic flexural resistance for the H_{max}, H_{min}, and H_{av} models increased by about 42%–72%, 51%–61%, and 9%, respectively, with an increase of the thickness of the joints (from T270 to T300 group). The maximum rotations for the C300, C270, and C240 groups decreased by about 3%, 18%, and 4%, respectively, with an increase in H from H_{min} to H_{max}. The maximum rotations for the H_{min} and H_{av} model groups increased by about 18%–25% and 26%–39%, respectively, with an increase of the thickness of the joints (from C270 to C300 group).

Meanwhile, the maximum rotation for the H_{max} model decreased by about 21%–41% with an increase of the thickness of the joints (from C270 to C300 group). Generally, the maximum rotation decreased with an increase in H from H_{min} to H_{max}. The rotation capacities for the H_{min} and H_{av} model groups increased by about 9%–23% and 20%–23%, respectively, with an increase of the thickness of the joints (from C270 to C300 group). Meanwhile, the rotation capacities for the H_{max} model decreased by about 23%–41% with an increase of the thickness of the joints (from C270 to C300 group). The Ψ_j (the joint ductility) values for the C300, C270, and C240 groups increased by about 15%–54%, 86%, and 59%–67%, respectively, with an increase in H from H_{min} to H_{max}. The Ψ_j values for the H_{max} and H_{min} models decreased by about 56%–83% and 43%–50%, respectively, with an increase in the thickness of the web and flange in the C240 to C300 web cleat joints. Meanwhile, the Ψ_j values for the H_{av} model increased by about 13%–80% with an increase of the thickness of the joints (from C270 to C300 group). The $\Psi_{j.max.load}$ (the rotation values at the maximum load and corresponding ductility) values for the C300, C270, and C240 groups increased by about 18%–54%, 86%, and 59%–70%, respectively, with an increase in H from H_{min} to H_{max}. The $\Psi_{j.max.load}$ values for the H_{max} and H_{min} models decreased by about 54%–83% and 41%–48%, respectively, with an increase of the thickness of the joints (from C270 to C300 group). Meanwhile, the $\Psi_{j.max.load}$ values for the H_{av} model increased by about 19%–81% with an increase of the thickness of the joints (from C270 to C300 group). The energy dissipations for the C270, and C240 groups increased by about 15%–40%, respectively, with an increase in H from H_{min} to H_{max}. Meanwhile, the energy dissipations for the C270 model decreased by about 33.33% with an increase with an increase in H from H_{min} to H_{max}. The energy dissipations for the H_{min} and H_{av} models increased by about 23%–39%, respectively, with an increase of the thickness of the joints (from C270 to C300 group). Meanwhile, the energy dissipations for the H_{max} model decreased by about 26%–37% with an increase of the thickness of the joints (from C270 to C300 group).

5. Failure Modes and Strain

Fig. 5 shows the moment–strain responses for the nine full-scale specimens of steel-bolted connections with web cleat joints in all groups. According to these curves, there is a correlation between the moment-rotation and moment–strain curves of both tools, which can be taken as further proof of the installation and measurement precision. As can be observed in Fig. 5, at the point of failure for each specimen, all of the strains changed from elastic to plastic for the three groups of specimens. There are three failure modes in the Eurocode 3 for the web cleat connections. Mode 1 is the complete flange yielding without bolt failure. Mode 2 is the flange yielding with bolt failure, and Mode 3 is the bolt failure. The failure modes were observed during the tests: the bolt being directly overloaded by the applied forces on the beam of the Web cleat connection (Mode 3) (Fig. 6). The failure modes of the specimens appeared after necking positions on the beam of the Web cleat connection (Fig. 6).

6. Conclusions

In this study, new connection types were suggested, and their behaviors were determined using full-scale experiments. T-shaped combinations created using the IPE standard profile and T-shaped elements are different from those in the literature, which utilize welded plates. Thus, the elimination of the problems occurring at the welds of connections such as the occurrence of fracture points and the inability to perform well in place is expected. To recommend the use of weld-less T connections, a knowledge of their behavior is needed. However, web cleat connections that use the IPE standard profile are not mentioned and investigated in either Eurocode 3 or the literature, as in this research. Thus, the aim of this study was to analyze the influence of T connections that utilize the IPE standard profile and the height of beam to height of web cleat joint (H) of web cleat joints on the behaviour of steel connections, to provide the necessary data for improving Eurocode 3 and efficiently use residue IPE standard profiles, rather than send them back to the consumption cycle. The main conclusions can be summarized as follows:

- The resistance moment increased with an increase in H from H_{min} to H_{max}.
- The resistance moment increased with the increase in the thickness of the web and flange in the C240 to C300 web cleat joints.
- The rate of the initial stiffness to the post-limit stiffness increased with an increase in the H from H_{min} to H_{max}.
- The rates of the initial stiffness to the post-limit stiffness for the H_{max} and H_{av} model groups increased with an increase of the thickness of the joints (from C270 to C300 group). The rotations of the plastic flexural resistance and the maximum rotations decreased with an increase in H from H_{min} to H_{max}.
- The rotations of the plastic flexural resistance increased with an increase of the thickness of the joints (from C270 to C300 group).
- The maximum rotations and the rotation capacities for the H_{min} and H_{av} model groups increased with an increase of the thickness of the joints (from C270 to C300 group).

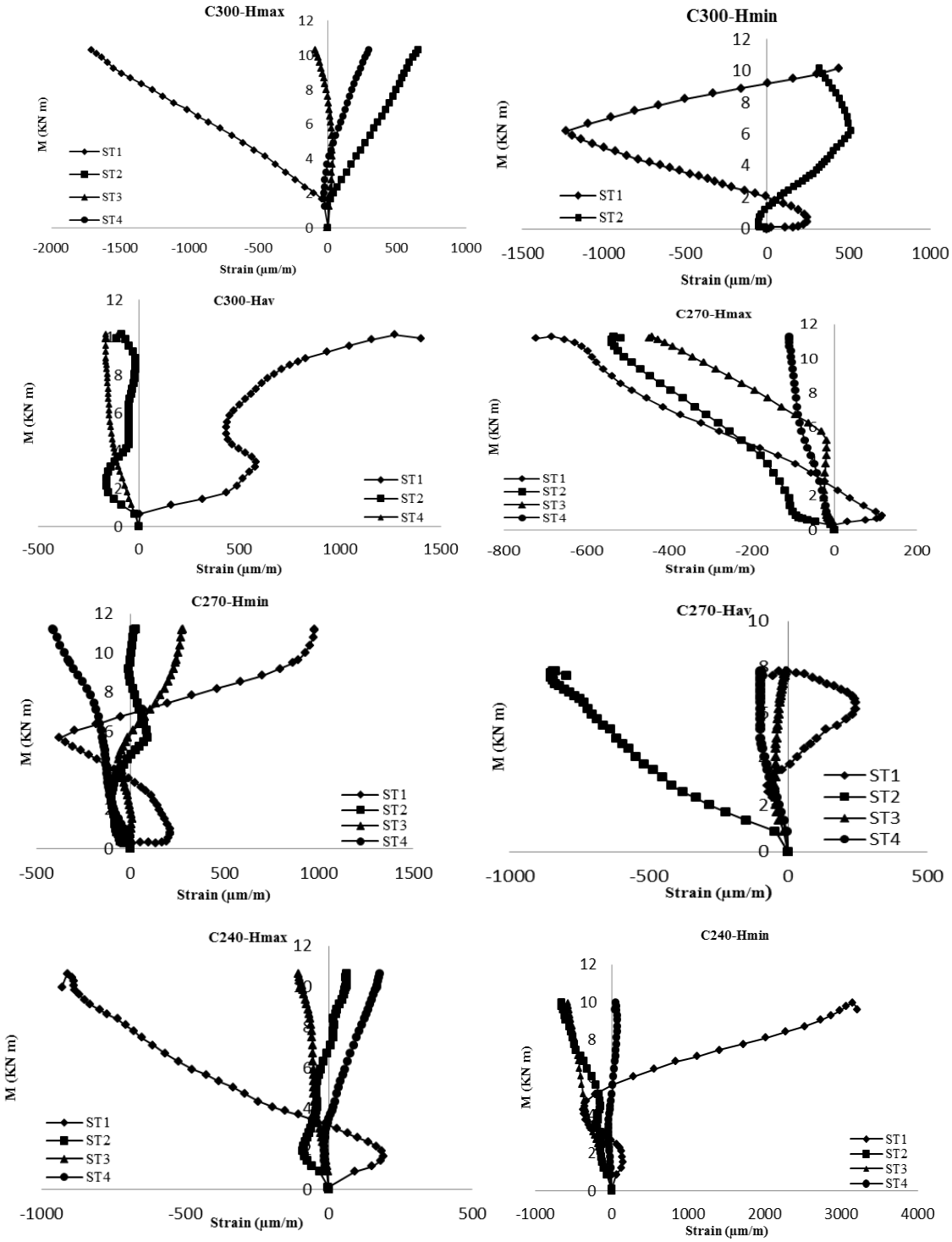

Fig. 5. Moment–strain curves.

- The Ψ_j (the joint ductility) values and the $\Psi_{j.max.load}$ (the rotation values at the maximum load and corresponding ductility) values increased with an increase in H from H_{min} to H_{max}.
- The Ψ_j (the joint ductility) values and the $\Psi_{j.max.load}$ (the rotation values at the maximum load and corresponding ductility) values for the H_{max} and H_{min} models decreased with an increase of the thickness of the joints (from C270 to C300 group). Meanwhile, the Ψ_j (the joint ductility) values and the $\Psi_{j.max.load}$ (the rotation values at the maximum load and corresponding ductility) values for the H_{av} model increased with an increase of the thickness of the joints (from C270 to C300 group). Thus, the model with H_{av} was ideal model.
- The energy dissipations for the C270, and C240 groups increased with an increase in H from H_{min} to H_{max}. Meanwhile, the energy dissipations for the C270 model decreased with an increase with an increase in H from H_{min} to H_{max}. The energy dissipations for the

H_{min} and H_{av} models increased with an increase of the thickness of the joints (from C270 to C300 group). Meanwhile, the energy dissipations for the H_{max} model decreased with an increase of the thickness of the joints (from C270 to C300 group).

- The failure modes were observed during the tests: the bolt being directly overloaded by the applied forces on the beam of the Web cleat connection (Mode 3). The failure modes of the specimens appeared after necking positions on the beam of the Web cleat connection.

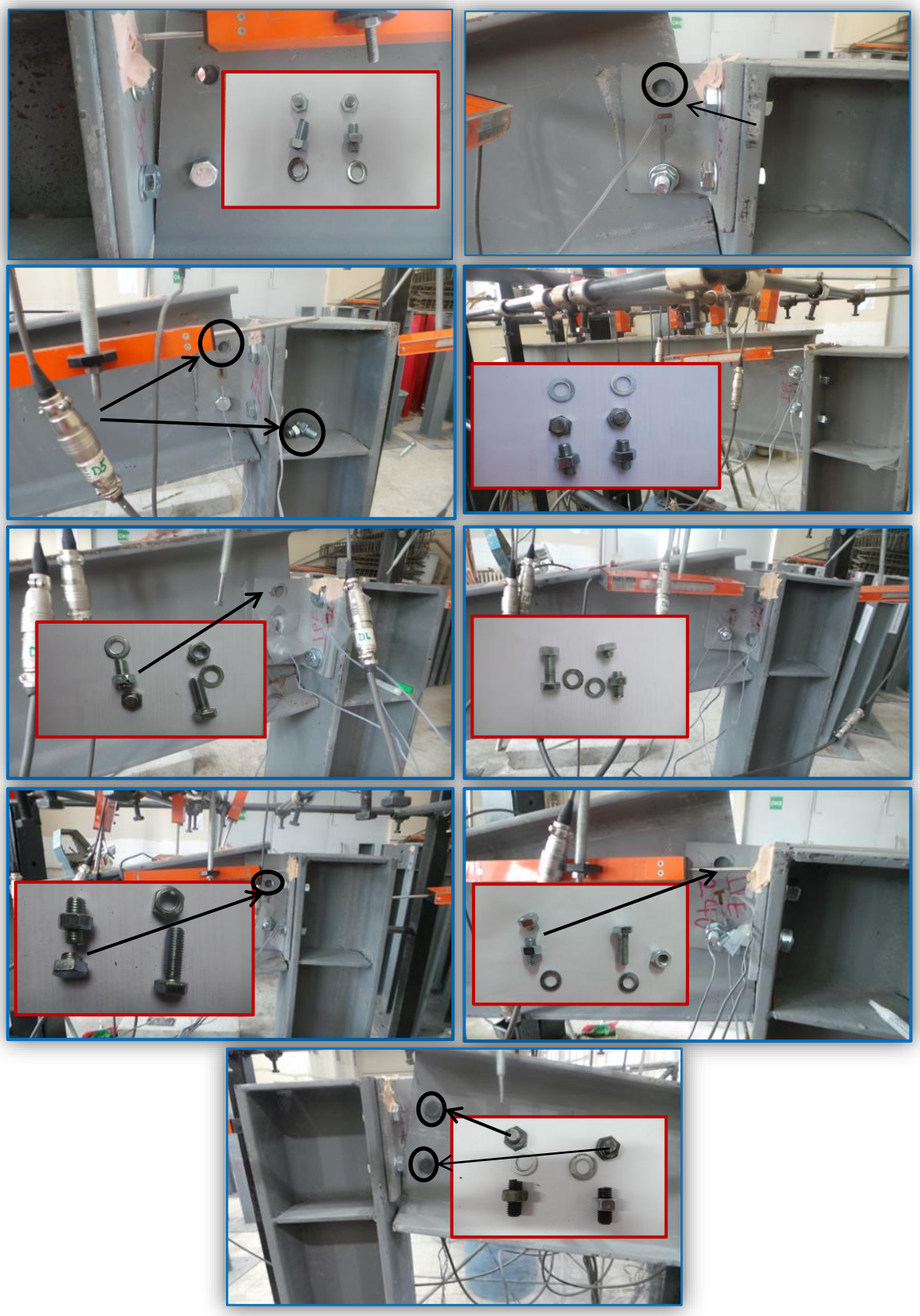

Fig. 6. Failure of models.

Acknowledgements

The writers gratefully acknowledge the financial support given by the BAP project (2015/126) of Ataturk University and the financial support given by the TÜBİTAK (2215) for Mahyar Maali and the support provided by the Gençler Metal steel company in making test specimens available. Their support in conducting the tests is most appreciated.

References

Aydın AC, Kılıç M, Maali M, Sağıroğlu M (2015a). Experimental assessment of the semi-rigid connections behavior with angles and stiffeners. *Journal of Constructional Steel Research*, 114, 338–348.

Aydın AC, Maali M, Kılıç M, Sağıroğlu M (2015b). Experimental investigation of sinus beams with end-plate connection. *Thin-Walled Structures*, 97, 35–43.

CEN (2005). Design of steel structures. Part 1.8: Design of joints, Stage 49 draft. European Committee for Standardization, Brussels.

Coelho AMG, Bijlaard FSK, Gresnigt N, Silva LS (2004). Experimental assessment of the behaviour of bolted T-stub connections made up of welded plates. *Journal of Constructional Steel Research*, 60, 269–311.

EN10002-1 (2001).Metallic materials– tensile testing–part 1: Method of testing at ambient temperature. European Standard, CEN, Brussels.

Fatemi SM, Showkati H, Maali M (2013). Experiments on imperfect cylindrical shells under uniform external pressure. *Thin-Walled Structures*, 65, 14–25.

Gil B, Cabrero JM, Goñi R, Bayo E (2003). An assessment of the rotation capacity required by structural hollow sections for plastic analysis. In: Jaurrieta MA, Alonso A, Chica JA (ed) *Tubular Structures*, A.A. Balkema Publishers, X. Lisse Holland, 277–292.

Lima LRO, Andrade SAL, Vellasco PCGS, Silva LS (2002). Experimental and mechanical model for predicting the behavior of minor axis beam-to-column semi-rigid joints. *International Journal of Mechanical Sciences*, 44, 1047–1065.

Maali M, Aydın AC, Sağıroğlu M (2015). Investigation of innovative steel runway beam in industrial building. *Sadhana - Academy Proceedings in Engineering Sciences*, 40, 2239–2251.

Maali M, Kılıç M, Sağıroğlu M, Aydın AC (2016). Experimental model of the behavior of bolted angles connections with stiffeners. *International Journal of Steel Structures*, 16(3), 719–733.

Maali M, Kılıç M, Sağıroğlu M, Aydın AC (2017). Experimental model for predicting the semi-rigid connections' behaviour with angles and stiffeners. *Advances in Structural Engineering*, 20(6), 884–895.

Maali M, Kılıç M, Yaman Z, Ağcakoca E, Aydın AC (2019). Buckling and post-buckling behavior of various dented cylindrical shells using CFRP strips subjected to uniform external pressure: Comparison of theoretical and experimental data. *Thin-Walled Structures*, 137, 29–39.

Maali M, Sagiroglu M, Solak MS (2018). Experimental behaviour of screwed beam-to-column connections in cold-formed steel frames. *Arabian Journal of Geosciences*, 11(9), 205.

Maali M, Showkati H, Fatemi SM (2012). Investigation of the buckling behavior of conical shells under weld-induced imperfections. *Thin-Walled Structures*, 57, 13–24.

Niloufari A, Showkati H, Maali M, Fatemi SM (2014). Experimental investigation on the effect of geometric imperfections on the buckling and post-buckling behavior of steel tanks under hydrostatic pressure. *Thin-Walled Structures*, 74, 59–69.

Piluso V, Rizzano G (2008). Experimental analysis and modeling of bolted T-stubs under cyclic loads. *Journal of Constructional Steel Research*, 64(6), 655–669.

Sağıroğlu M, Aydin AC (2015). Design and analysis of non-linear space frames with semi-rigid connections. *Steel and Composite Structures*, 18(6), 1405–1421.

Sagiroglu M, Maali M, Kılıç M, Aydın AC (2018). A novel approach for bolted T-Stub connections. *International Journal of Steel Structures*, 18(3), 891–909.

SB EN ISO 898-1:1999 (2009). Mechanical properties of fasteners made of carbon steel and alloy steel: Bolts, screws and stud. (Published: October 1999 Replaced By: SB EN ISO 898-1:2009, Revised, Withdrawn)

Schleich JB, Chantrain P, Chabrolin B, Galéa Y, Bureau A, Anza J, Espiga F (1998). Promotion of plastic design for steel and composite cross sections: New required conditions in Eurocodes 3 and 4, practical tools for designers. European Commission, Luxembourg.